ACS APPLIED NANO MATERIALS

www.acsanm.org Article

Hafnium Oxide/Graphene/Hafnium Oxide-Stacked Nanostructures as Resistive Switching Media

Tauno Kahro,* Aivar Tarre, Tanel Käämbre, Helle-Mai Piirsoo, Jekaterina Kozlova, Peeter Ritslaid, Aarne Kasikov, Taivo Jõgiaas, Guillermo Vinuesa, Salvador Dueñas, Helena Castán, Aile Tamm, and Kaupo Kukli

Cite This: https://doi.org/10.1021/acsanm.1c00587 Read Online

ACCESS | Metrics & More | Article Recommendations

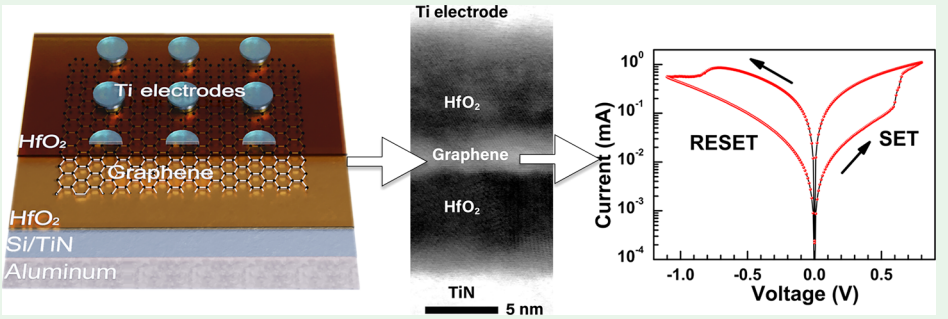

ABSTRACT: Thin HfO_2 films were grown by atomic layer deposition on chemical vapor-deposited large-area graphene. The graphene was transferred, prior to the deposition of the HfO_2 overlayer, to the HfO_2 bottom dielectric layer pregrown on the Si/TiN substrate. Either $HfCl_4$ or $Hf[N(CH_3)(C_2H_5)]_4$ was used as the metal precursor for the bottom layer. The O_2 plasma-assisted process was applied for growing HfO_2 from $Hf[N(CH_3)(C_2H_5)]_4$ also on the top of graphene. To improve graphene transfer, the effects of the surface pretreatments of the as-grown and aged Si/TiN/HfO_2 substrates were studied and compared. The graphene layer retained its integrity after the plasma processes. Studies on resistive switching on HfO_2-graphene-HfO_2 nanostructures revealed that the operational voltage ranges in the graphene-HfO_2 stacks were modified together with the ratios between high- and low-resistance states.

KEYWORDS: *graphene, atomic layer deposition, hafnium oxide, stacked nanostructures, resistive switching*

INTRODUCTION

Metal oxide−graphene-based memristor switches have emerged as attractive and promising devices due to the possibility to downscale both switchable medium thickness and effective electrode area, together with further integration of the memory matrices with flexible substrates.[1,2] Graphene may be used as an interfacial barrier layer controlling ionic transport between metal oxide-based medium and the electrode metal. The latter was proposed in a study by Lee et al., conducted on Ta/graphene/Ta_2O_5 stacks.[3] The performance models of resistively switching devices have been presented and schematized in numerous studies on material stacks constituting such devices, including those containing graphene.[1−3] Graphene has also been used in HfO_2-based resistive switching memory stacks as a complementary conducting layer between HfO_2 and top metal electrodes,[4] or, as an interesting alternative, in the form of the edge electrode in contact with HfO_2-based switching medium.[1] In the former study,[4] graphene layers were mounted between the HfO_2 surface and top electrodes made of inert gold metal, in order to provide an effective oxygen reservoir at the oxide−metal interface.

Graphene layers are most commonly formed using H_2-assisted pyrolysis of methane, CH_4, via high-temperature chemical vapor deposition (CVD) on catalytic metal (Cu and Ni) substrates and thereafter transferred to the functional insulator substrates. It is important to note that the transfer procedure of CVD-grown graphene is commonly carried out at room temperature, which allows one to rely on the safety of the procedure in terms of its possible influence on the structure and composition of substrate layers. At the same time, if another functional insulator layer is to be deposited from the

Received: February 26, 2021
Accepted: May 3, 2021

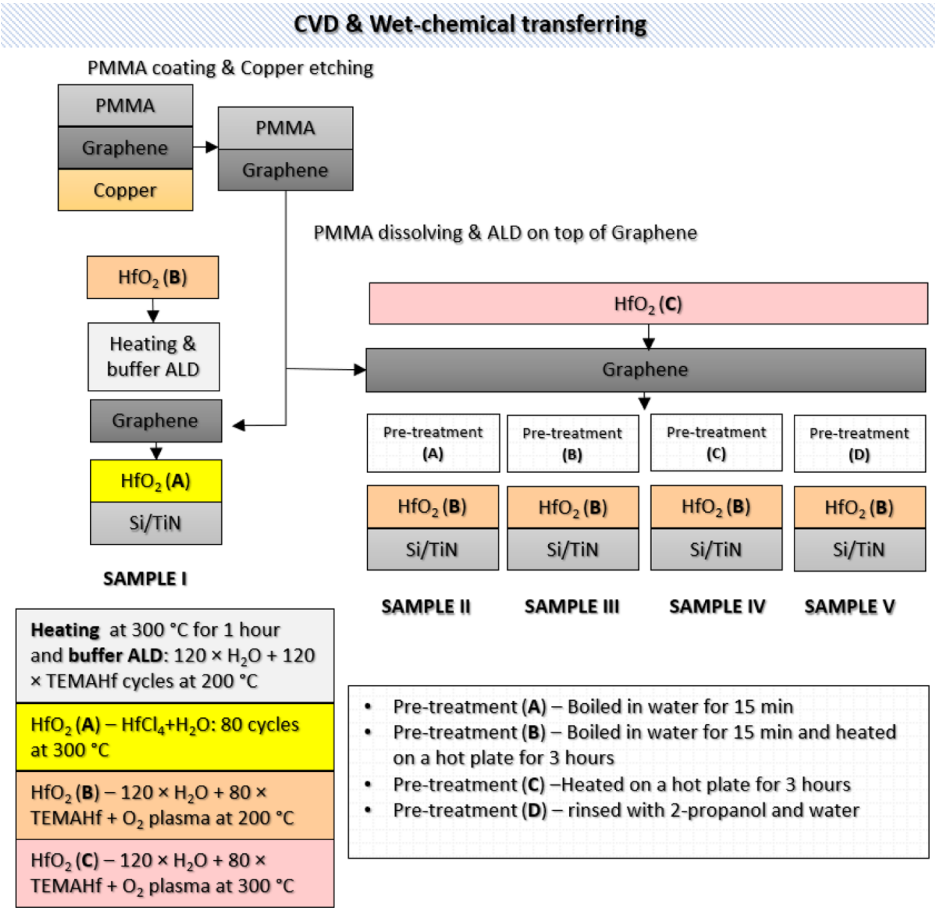

Figure 1. Schematic representation of the preparation process of the stacked nanostructures.

vapor phase on the transferred graphene, then one has to beware that the deposition process, which has often had to be carried out at elevated temperatures and using aggressive reactants, may, at first, distort or even destroy the integrity of the graphene layers. In this connection and if the goal is to build a functional device structure, such as a resistively switching cell, in consecutive processes demanding elevation of substrate temperatures and exploitation of, for example, plasma-assisted deposition, it would be imperatively necessary to thoroughly study the effect of such a sequence of processes on the quality of the transferred graphene.

Direct growth of graphene on, for example, metal oxide substrates remains a challenge, and advancing of wet chemical transfer processes is still in order. Feasible deposition of dense dielectric metal oxides on graphene has also been a well-known issue along with the development of graphene-based junctions. Application of various metal precursor chemistries, reactor parameters, seed layers, and different graphene functionalization procedures has been examined.[2,5−8] Atomic layer deposition (ALD) has herewith been applied in the wafer-scale fabrication of HfO_2 gate dielectrics for graphene channel transistors, whereby the HfO_2 films were grown using $Hf[N(CH_3)(C_2H_5)]_4$ (TEMAHf) and H_2O as precursors at 200 °C.[9] Later, it has been reported that HfO_2 films can be grown by ALD from TEMAHf and H_2O even at 120 °C on the graphene transistor channel, providing better defined device performance compared, for example, to the ALD-grown TiO_2 and Al_2O_3 gate dielectrics.[10]

Application of TEMAHf in the ALD process[11] could nowadays be regarded as a part of possibly the most feasible route to HfO_2 films on graphene.[9,10,12−16] Other hafnium alkylamides such as $Hf[N(CH_3)_2]_4$[17,18] are also of interest because application of alkylamide-based precursor chemistry allows one to exploit rather low substrate temperatures in the range of 100−200 °C. Low temperatures effectively assist in increasing the nucleation density of films on carbon substrates.[14]

Complementary procedures can be applied in order to create and increase the density of nucleation sites on otherwise inert graphene. Electron-beam irradiation has reported to be useful on the graphene surface prior to ALD of HfO_2 at 90 °C from $Hf[N(CH_3)_2]_4$.[18] Ion-beam-assisted treatment has been examined as a procedure assisting in removal of PMMA residues after the graphene transfer procedures and before ALD of HfO_2 at 200 °C. Atmospheric oxygen plasma treatment of graphene has been described as a useful procedure for increasing the nucleation density of thin ZrO_2 films upon ALD at 150 °C from $Zr[N(CH_3)(C_2H_5)]_4$.[19] The latter is worth noting because of the similarity between Zr and Hf precursor chemistries and the crystalline structure of ZrO_2 and HfO_2.

Carbon-free $HfCl_4$ can be exploited as the hafnium precursor, providing crystal growth in HfO_2 films in the deposition temperature range of 220−750 °C.[20] $HfCl_4$ is resistant to thermal decomposition and can thus be applied in a much wider substrate temperature range compared to the metal alkylamide precursors. The application of $HfCl_4$ for the

https://doi.org/10.1021/acsanm.1c00587
ACS Appl. Nano Mater. XXXX, XXX, XXX−XXX

ALD of HfO_2 on the top of graphene has earlier required prefunctionalization of graphene by growing the first HfO_2 layers on graphene from $HfCl_4$ and H_2O at a temperature as low as 180 °C,[21] that is, at substrate temperatures reduced below those otherwise considered as those optimized for the given precursor system. Later, another study has been carried out to comparatively investigate the growth of HfO_2 films on graphene by ALD from $Hf[N(CH_3)(C_2H_5)]_4$ and $HfCl_4$ at 250 °C.[22] In the latter study, the structural and electrical properties of the oxide grown in chloride-based ALD were actually claimed as superior, compared to those evaluated after the alkylamide-based ALD. Nevertheless, it is worth noting that the exploitation of the TEMAHf precursor may also allow crystallization, that is, growth of HfO_2 with an ordered structure at temperatures as low as 250 °C, when deposited using O_2 plasma as the oxygen precursor.[23]

HfO_2-graphene-HfO_2 nanostructures with graphene embedded between HfO_2 host layers have seldom been publicly described to date. Few studies have employed either graphene oxide nanodots[24] or graphene platelets (domains)[25] as electron traps inside the HfO_2 insulator dielectric films, in order to engineer charge trapping memory cells.

HfO_2 is an ionic metal oxide which inevitably contains its metastable polymorphs and oxygen vacancies in its as-deposited state. At the same time, HfO_2 essentially crystallizes as dioxide, instead of suboxides. Besides inherent chemical stability, ALD of HfO_2 has been scaled up well enough in terms of the selection of precursor chemistry, reactor design, and deposition temperatures for processes on noncarbon substrates. HfO_2 is also a material partially accommodated to contemporary nanoelectronics whereby hafnium alkylamides, such as TEMAHf, are prospective chemicals, generally providing dense nucleation and growth of uniform nanolayers. In regard with the application of plasma-assisted growth, the influence of plasma on graphene-based substrate structures is yet to be described in the case of the present precursor chemistry and pretreatments, which is also one of the goals of the present study.

The present study is devoted to the examination of the feasibility of graphene transfer routes from the catalyst copper substrate onto HfO_2 films grown by ALD in either $HfCl_4$ or $Hf[N(CH_3)(C_2H_5)]_4$-based process. The graphene layers were afterward embedded between HfO_2 films, whereby the HfO_2 layers covering the graphene were grown by ALD using $Hf[N(CH_3)(C_2H_5)]_4$ and O_2 plasma as precursors. Spectroscopic and microscopic studies were subsequently conducted in order to evaluate possible affection of the plasma-assisted ALD on graphene. The performance of the HfO_2-graphene-HfO_2 nanostructures as resistive switching media was evaluated as a functional application of the engineered stacks.

EXPERIMENTAL SECTION

Sample Preparation. Graphene was grown on commercial 25 μm-thick polycrystalline copper foil (99.5%, Alfa Aesar) in an in-house-built CVD reactor. The foil was annealed, prior to the graphene deposition, at 1000 °C in Ar/H_2 (99.999%, Linde Gas) flow for 60 min and then additionally exposed to the mixture of 10% CH_4 (99.999%, Linde Gas) in Ar at 1000 °C for 120 min. Then, the foil was cooled down in Ar flow.

The graphene was transferred from copper foils onto reference Si/SiO_2 and $Si/TiN/HfO_2$ substrates using a wet transfer process. Poly(methyl-methacrylate) (PMMA, with a molecular weight of ~996,000 g/mol, Sigma-Aldrich) was dissolved in chlorobenzene (Sigma-Aldrich) and then spin-coated onto one side of the graphene/Cu/graphene structures with a thickness of around 120 nm, and the graphene on the uncoated side was removed by plasma treatment. The Cu foil was dissolved in 1 M $(NH_4)_2S_2O_8$ solution overnight. To remove the residual etchant, the floating PMMA/graphene film was soaked several times in deionized water baths and transferred onto differently treated substrates (Figure 1). The samples were dried in air for 20 h and then heated on a hot plate at 100 °C for 1 h to improve the contact between graphene and the substrate. The PMMA layer was removed by dissolving it in dichloromethane (Sigma-Aldrich). Finally, graphene samples were rinsed with 2-propanol.

For the deposition of HfO_2 films, two ALD routes were used, distinctive on the basis of the precursor chemistry. $HfCl_4$ and TEMAHf were applied as metal precursors. $HfCl_4$ was, in the present study, considered as a carbon-free precursor effectively providing growth of HfO_2 films together with crystallization. O_2 plasma was exploited as the oxygen precursor together with TEMAHf. For the deposition of the first HfO_2 layer directly on the bottom TiN electrode as for the substrate to the subsequently transferred graphene, both $HfCl_4$ and TEMAHf were used as the metal precursor in separate experiments (Figure 1), whereas for the growth of the HfO_2 film on the top of the graphene layer, only the TEMAHf-based process was exploited. In order to form the base stack structure as a substrate for the further transfer of graphene domains, the HfO_2 films were grown either at 300 °C, by applying 80 ALD cycles with $HfCl_4$ and H_2O as precursors (Figure 1, Sample **I**), or at 200 °C, by first applying 120 pulses of H_2O followed by 80 ALD cycles consisting of alternate TEMAHf and O_2 plasma pulses (Figure 1, Samples **II**–**V**).

HfO_2 films were deposited from $HfCl_4$ and H_2O in an in-house-built hot-wall flow-type ALD reactor.[26] ALD of HfO_2 from $Hf[N(CH_3)(C_2H_5)]_4$ and remote O_2 plasma was carried out in a commercial Picosun R-200 Advanced ALD system. The bottom electrode substrates exploited were pieces of Si wafers that had been coated with a conductive and crystalline 10 nm-thick TiN layer. TiN was grown by pulsed CVD using a batch $TiCl_4/NH_3$ process[27,28] at temperatures of 450–500 °C in an ASM A412 Large Batch 300 mm reactor at Fraunhofer IPMS-CNT.

Different surface treatment procedures were applied before completion of the switching stack devices. The description of procedures together with their possible effects on structural quality of graphene and metal oxide layers will fully be described below in order to allow one to decide on the necessity to apply these upon construction of functional, switchable nanodevices.

The CVD-grown graphene transferred to an as-deposited ALD-HfO_2 tended to roll off, wrinkle, and break, not adhering to the metal oxide layer. It is worth noting that the transfer process of the graphene could be improved, resulting in an appreciably homogeneous and reliable adhesion of the graphene domains on the HfO_2 film surface. The adhesion was strengthened after storing the HfO_2-covered substrates under laboratory air conditions over several days, sealed against sticking of dust particles, but open to humidity. After storage of HfO_2 in an air environment over 160 h, approximately, the graphene transferred onto the HfO_2 surface was adhered appreciably, without delamination, as observed in the case of Sample **I** (Figure 1). The observation implied the need for controlled pretreatment of the as-deposited oxide surface. For this, various substrate treatments before graphene transfer can be found in the literature. For Si/SiO_2 substrates, to increase hydrophilicity (for instance, to increase the density of OH groups), HF dip or plasma treatment could be used.[29] On the other hand, different substrate treatments will create the number of charged defects and could have a negative effect of fabricated graphene devices (for instance, mobility of charge carriers could decrease).[29,30] For ALD-grown dielectrics, plasma treatment may reactivate the surfaces of objects. Therefore, milder surface treatment techniques, such as water, alcohols, or heating prior to the graphene transfer procedure, could be used to replace too aggressive treatments, as also shown in Figure 1, Samples **II**–**V**.

The growth of HfO_2 films on the top of graphene also required pretreatment of the substrate surface, as noted above. The top HfO_2 layer was grown on transferred graphene using TEMAHf and O_2 plasma in all cases. For the graphene on HfO_2 grown from $HfCl_4$ and

https://doi.org/10.1021/acsanm.1c00587
ACS Appl. Nano Mater. XXXX, XXX, XXX–XXX

H_2O (Sample **I**, Figure 1) prior to the growth of top HfO_2, the surface of graphene was preheated at 300 °C for 1 h to clean its surface from possible residues and then exposed to 120 sequential H_2O pulses followed by 120 TEMAHf pulses at 200 °C. The latter treatment was, at first, applied in order to prepare the graphene substrate by covering it by a disordered oxide layer, assumptionally providing fast nucleation of the functional HfO_2 film. Additionally, the purpose of the treatment was to protect the graphene against the possible damaging effect of O_2 plasma via pregrowth of a buffer layer by applying a water-assisted procedure. All the samples were exposed to an additional sequence of 120 H_2O pulses before the growth of the top HfO_2 layer, in order to ensure the preoxidation of the buffer layer and protection of graphene. The HfO_2 film on the top was, thereafter, formed by applying 80 HfO_2 cycles consisting of a sequence of 0.3−4.0 to 15.0−4.0 s for TEMAHf pulse-purge-O_2 plasma pulse-purge, respectively, either at 200 °C (Sample **I**, Figure 1) or at 300 °C (Samples **II**−**V**, Figure 1). Similar reference HfO_2 structures were prepared using two different ALD chemistries but without graphene embedded in HfO_2.

Characterization. Structural characterization of graphene-based nanostructures was performed using a micro-Raman spectroscopic system Renishaw inVia at an excitation wavelength of 514 nm, that is, the excitation energy was 2.4 eV. The spectral resolution reached, approximately, 1.5−2 cm^{-1}. The Si reference was used for calibration.

The surface morphology of the graphene and HfO_2 films was evaluated by high-resolution scanning electron microscopy (HR-SEM; FEI Helios NanoLab 600). The focused ion beam (FIB; FEI Nanolab 600 dual-beam (SEM-FIB) system) in situ lift-off technique was used to prepare thin samples for high-resolution transmission electron microscopy (HR-TEM) study. TEM analysis was performed in the scanning mode (STEM) at 200 kV using a Cs-probe-corrected transmission electron microscope (FEI Titan Themis 200). The thickness and crystal structure of the deposited HfO_2 films were evaluated by X-ray reflectometry and by grazing incidence X-ray diffractometry (GIXRD), respectively, using Cu Kα radiation (SmartLaB, Rigaku).

The X-ray photoelectron spectroscopy (XPS) spectra were collected at normal emission using a Gammadata/Scienta SES100 hemispherical analyzer and a Thermo VG Scientific XR3E2 nonmonochromatized dual anode X-ray source (Al Kα/Mg Kα). The analyzer energy scale calibration was checked against the $4f_{7/2}$ line from cleaned gold foil at 84.0 eV binding energy. Relevant to estimating elemental composition from XPS survey scans, the constant (i.e., independent of photoelectron kinetic energy) analyzer transmission function was checked against accessible core level lines of clean Au, Ag, and Cu samples and additionally asserted by constant magnification in spatial imaging (in the nonenergy-dispersive direction) of a structured test sample through the electron optics over the entire used kinetic energy range. The minor sample charging was corrected for by adjusting the adventitious carbon (typically present in ex situ-measured samples) C 1s peak to 284.8 eV. Spectral components were fitted, and elemental content from survey spectra was estimated using CasaXPS software,[31] used for the quasi-metallic graphene sp^2 component appropriate asymmetric lineshapes[32] to conservatively estimate the relative contributions from impurity carbon species (sp^3 carbon- and oxygen-bonded). The overlayer graphene C 1s analysis was further checked and refined using the SPANCF package.[33,34]

Optical measurements of the graphene nanostructures were performed on spectroscopic ellipsometer GES-5E (Semilab Co) using a microspot option where light is focused on a film surface via a telescope. The converging angle of a beam was about 4°, and the spot size was about 0.35 × 0.8 mm for 65° angle of incidence. Fitting was performed using the program SEA and Tauc-Lorentz dispersion model. Fit quality was characterized using a correlation function between the measured and computed spectra R^2.

For the electrical measurements, HfO_2-graphene-HfO_2 stack structures were supplied with titanium electrode electron beam evaporated to thicknesses of 100−110 nm through a shadow mask at 230 °C. Backside contact to the measurement circuitry was provided by the thermally evaporated aluminum layer with a thickness of 100 nm at room temperature. Electrical measurements were carried out in a probe station. The Ti electrodes used in the measurement had either a diameter of 50 μm (area 0.002 mm^2) or 250 μm with an area of 0.05 mm^2. The samples were electrically characterized in both dc and ac regimes using a Keithley 4200 SCS semiconductor analyzer. The bias voltage was applied to the top electrode, while the bottom electrode was grounded. The forming procedure was carried out as a voltage sweep with positive bias, and a current compliance in the order of microamperes was applied to avoid irreversible breakdown of devices. In general, the formation took place between 1.5 and 4 V. The current−voltage curves were obtained by applying positive and negative voltage sweeps, while the memory maps were measured by applying increasing voltage pulses while maintaining a reading voltage of 0.1 V.

RESULTS AND DISCUSSION

Morphology and Structure. According to SEM analysis, the as-transferred graphene was appreciably uniform and the film coverage was, as estimated, more than 95%. It should be mentioned that for the as-grown HfO_2 dielectrics, only boiling in deionized water and then heating in a hot plate improve graphene transfer, whereas 2-propanol-rinsed samples showed more breaks and cracks. Furthermore, graphene layers on aged, that is, openly stored, ALD dielectrics became similar, in terms of continuity, to those on HfO_2 in Sample **I** and implied no clear dependence on the selected pretreatments.

In the image of transferred graphene on the Si/TiN/HfO_2 substrate (Figure 2a), one can see wrinkles, which may have resulted from the transferring process. The structure and morphology of the bottom HfO_2 dielectric layer were similar in all cases regardless of the precursor used. The morphology

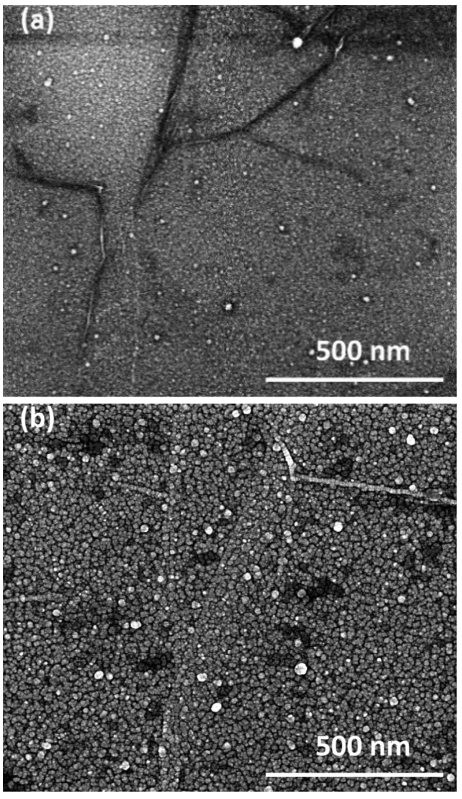

Figure 2. SEM images of (a) Si/TiN/HfO_2/graphene (Sample **IV** before the top HfO_2 layer) and (b) Si/TiN/HfO_2/graphene/HfO_2 nanostructures (Sample **IV**).

https://doi.org/10.1021/acsanm.1c00587
ACS Appl. Nano Mater. XXXX, XXX, XXX−XXX

and/or the film coverage of top-layer HfO_2 on Si/TiN/HfO_2 and Si/TiN/HfO_2/graphene substrates was also uniform.

The surfaces were uniformly covered by grain-like features with an average size of about 20 nm, as evaluated (with ImageJ software) on the bird-eye SEM images. However, some darker areas, possibly "valleys" on the top layer of HfO_2 grown on graphene, can be seen in Figure 2b, which may be due to the morphological effect, that is, adhesion can vary between graphene and the Si/TiN/HfO_2 substrate.

The HfO_2 films were grown to the thicknesses ranging from 7.5 to 9.0 nm on Si substrates, in accordance with the XRR analysis. The thicknesses of HfO_2 films deposited both below and on the top of the transferred graphene layers were 9 nm (on Si/TiN substrates), as evaluated by spectroscopic ellipsometry. Similar layer thicknesses were also seen in the TEM images (Figure 3).

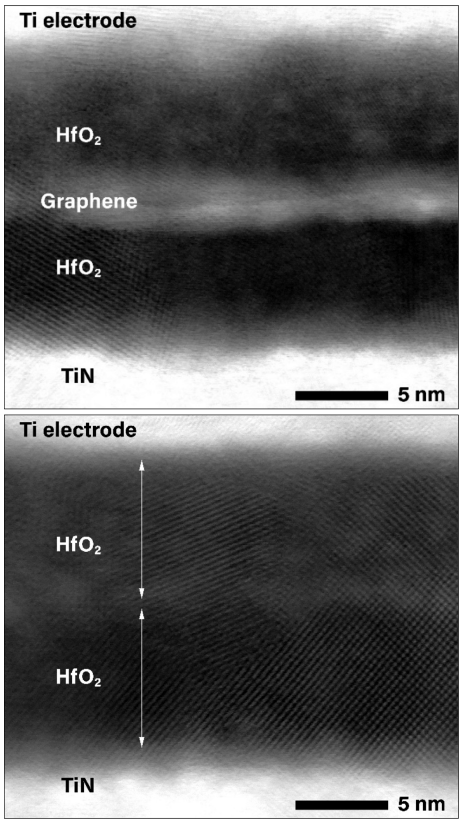

Figure 3. Cross-sectional high-resolution STEM bright-field image of the Si/TiN/HfO_2/graphene/HfO_2/Ti-electrode (Sample **I**, top) and Si/TiN/HfO_2/HfO_2/Ti-electrode (Sample **I** without graphene, bottom) stack structures.

TEM measurements showed that the different layers from the nanostructures are clearly distinguishable (Figure 3). The result visually resembles that earlier observed in the case of ZrO_2-graphene-ZrO_2 stacks[35] and in Ta-graphene-Ta_2O_5 stacks.[3] The top layer of HfO_2 both on graphene and on the bottom HfO_2 had a lower density as compared to the bottom HfO_2 film on the Si/TiN substrate. However, the top layer thickness was comparable to the bottom and both values were in accordance with the results of XRR and ellipsometry. Furthermore, the results showed that the HfO_2 films were at least partially crystallized, that is, possessed certain short-range ordering and nanocrystallinity.

The HfO_2 films grown on Si and Si/TiN substrate surfaces were formed as strongly disordered, that is, layers containing crystallites with a size of approximately 2 nm as estimated on the basis of GIXRD results (Figure 4) The diffractograms of

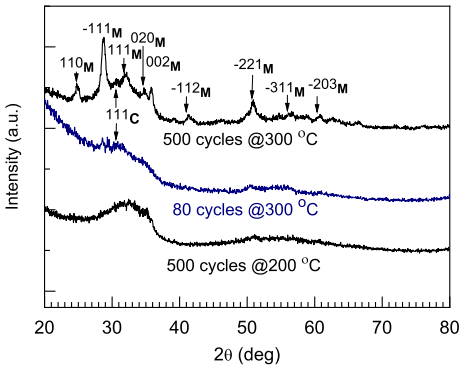

Figure 4. GIXRD patterns of HfO_2 films grown at different deposition temperatures with 80 and 500 growth cycles, indicated by labels. Miller indexes corresponding to the reflections of monoclinic (M) and cubic (C) polymorphs of HfO_2 are also indicated by labels.

the HfO_2 films grown from both TEMAHf and $HfCl_4$ precursors were similar. The results indicated that the first unambiguously identified reflections began to appear in the diffractograms from the films grown at 250 °C (not shown) and when using at least 500 growth cycles. In the latter, reference, the film was grown to a thickness of 50 nm, approximately, and the HfO_2 was crystallized in a dominantly monoclinic phase (card 34-0104), as revealed by reflections of moderate intensity but clearly apparent in the diffraction pattern. In the case of 80 growth cycles as used in the present work to deposit 7−9 nm-thick functional HfO_2 layers on TiN and on graphene, the growth of nanocrystals in the reference HfO_2 films was revealed only by weak and broad trace reflections at 28 and 30.3°, referring to the formation of metastable cubic polymorph of HfO_2 (card 96-900-9017) in addition to the stable monoclinic phase. In the reference films grown at 200 °C, implications of ordering became hardly detectable in the diffraction patterns.

Raman Spectroscopy. The Raman spectra of graphene transferred on the reference Si/SiO_2 substrate showed two main bands at 1587 cm^{-1} for G and at 2688 cm^{-1} for 2D bands (Figure 5). The positions of the bands slightly varied from sample to sample; therefore, the average values of each band position were used for further analysis. The 2D band had a narrow Lorentzian shape, which is one of the characteristic features of single-layer graphene.[36,37] The defect-related D band at 1350 cm^{-1} and the D′ band at 1620 cm^{-1} were initially absent in the Raman spectra, but they appeared after deposition of the upper HfO_2 dielectric layer on graphene either with or without "buffer ALD" treatments.

Positions of Raman bands characteristic of graphene varied on differently treated substrates, Figure 5, right panel. This shifting and widening of bands can be explained by strain[36] or more likely doping by charge transfer between graphene and the substrate,[38] which may be enhanced also by the inevitable presence of residual impurities. The position of the G band thus changes with (electron) doping. The frequency of the G band reaches its minimum value when the Fermi level is at the Dirac point. At room temperature, this value, ω_G, has been estimated to be 1579.2 cm^{-1},[36,39] and the Raman shift has

https://doi.org/10.1021/acsanm.1c00587
ACS Appl. Nano Mater. XXXX, XXX, XXX−XXX

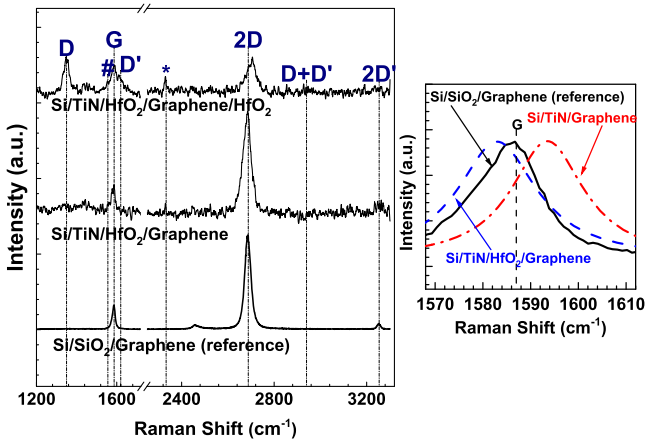

Figure 5. Representative Raman spectra of graphene-based stack structures in the case of differently stacked structures described by labels and normalized by the G band according to G band intensities where additional Raman bands at 1556 cm^{-1}, labeled by #, and those at 2333 cm^{-1}, labeled by *, indicate adsorbed oxygen and nitrogen molecules, respectively. The right panel represents Raman spectra normalized to the G band of the graphene-based stack structures in the energy range of 1570−1610 cm^{-1}.

increased with the concentrations of either holes or electrons.[40] The G band width has been reported to decrease symmetrically as the concentrations of electrons or holes increase.[36] The position of the 2D band also depends on the Fermi level, increasing with the hole concentration and decreasing with the electron concentration.[36,40] In addition, the integrated intensity of the 2D band has decreased as the Fermi level increases.[31]

Usually, CVD-grown graphene has been regarded as a slightly p-type conductor (i.e., hole doped due to the presence and charge transfer effect of oxygen and/or water).[40−43] In the present study, after transferring the CVD-graphene onto 7.5−9.0 nm-thick HfO_2 dielectric layers, downshifts of the positions and widenings of the G and 2D bands could be detected and measured, as shown in Figure 5. Similar behavior has recently been reported in a study by Ben Maad et al.,[41] where graphene was transferred on HfO_2 films of different thicknesses, and similar shifting and broadening of bands were measured, most prominent in the case of thinnest (5 nm) HfO_2 films. The high density of carriers transferred to graphene from such thin dielectrics (10 nm or less) may be explained by the localization of traps at the $Si/SiO_2/HfO_2$ interface but still closer to the graphene layer as compared to thicker dielectric layer/graphene structures.[41]

In the present study, the Raman measurements revealed that the positions of G and 2D bands reached the lowest values in the case where no water or other additional treatments were applied on the HfO_2 surface (deposited from $HfCl_4$) before the graphene transfer procedure (Figure 1, Sample **I**). It is thus indeed likely that either the pretreatment procedures conducted on the HfO_2 surface have covered the oxide with layers of chemical groups which at least partially blocked the charge transfer and accompanying the graphene doping process or HfO_2 deposited from TEMAHf has a lower amount of localized traps compared to the HfO_2 deposited from $HfCl_4$.

The treatment procedures with boiled water or 2-propanol on $Si/TiN/HfO_2$ substrates may have created a dense layer of hydroxyl groups on the dielectric surface, and therefore, the electron transfer (doping) from HfO_2 to graphene was at least partially hindered. Under such conditions, the significance of p-type doping may have increased somewhat, but still in lesser extents than in the case of the stacks consisting of graphene transferred to the Si/SiO_2 substrate.[44] It should be noted that, in accordance with the Raman results, the effect of the selected surface treatments on graphene on aged (i.e., openly stored under laboratory air conditions) HfO_2 dielectrics was weak, also showing similar (p-type) trends with implications of doping effects.

After the deposition of the top HfO_2 layers on graphene, the Raman signatures of graphene in the stacks became more uniform in terms of the positions and widths of G and 2D bands. The largest shift (22 cm^{-1}) in the location of bands has occurred in the case of HfO_2 grown in plasma-assisted ALD from TEMAHf on graphene transferred on HfO_2 grown from $HfCl_4$ (Sample **I**, Figure 1). However, after the deposition of the top HfO_2 layers, the positions of 2D bands increased rather than being decreased in terms of the frequency, being indicative of behavior opposite to the expected one, as the shift should presumably imply the increasing concentration of electrons and significance of n-doping. A possible explanation is that the HfO_2 films grown from $HfCl_4$ on TiN (Sample **I**, Figure 1) were additionally heated at 300 °C for 1 h, together with the transferred graphene layer. Upon heating at 300 °C, before the deposition of the upper HfO_2 layer, the surface of graphene was, probably, cleaned and more bonding sites for OH groups after H_2O treatment were provided, as proposed earlier in the literature.[45] The OH groups could further prevent electron doping from the upper-layer dielectric.[44] The result of the lesser extent of electron doping was a shift of the 2D band to higher frequencies, that is, higher significance of p-type doping, because OH groups can uptake electrons from graphene or HfO_2. In the cases of stacks, where the HfO_2 films were grown from TEMAHf and exposed to 120 H_2O pulses (Samples **II**−**V**, Figure 1), no extra heating was performed before 120 H_2O pulses. When the top layer of HfO_2 was deposited on graphene, similar Raman band shifts were observed, implying some significance of p-type doping. The shift from the initial positions, that is, from the positions recorded before the deposition of the top HfO_2 film on graphene, remained smaller than that in the case of Sample **I** (Figure 1).

To some extent, damaging graphene during the deposition of metal oxide layers on the top of graphene can hardly be avoided. In the present case, after the plasma-assisted ALD of the upper HfO_2 film, the D and D′ bands have emerged in the graphene Raman spectrum (Figure 5). The presence of these, generally defect-related, bands, D and D′ can mean either physical damage[46] or the exhibition of sp^3 hybridization[43,47,48] or be due to amorphous carbon complementarily formed on graphene.[49] In addition, the observed broadening of the Raman bands could also be a consequence of defects[50] or due to higher amplitudes of charge fluctuations ("puddles")[47] which could arise from charged impurities in the disordered dielectric layer and polar adsorbates (OH groups) between graphene and dielectrics.

On the other hand, the (larger) broadenings and (up and down) shifting of the bands could be an averaging effect over nanometer-scale strain variations.[51]

Interestingly, some Raman spectra (Figure 5) showed narrow bands at 1556 and 2333 cm^{-1}, which are probably indicative of O_2 and N_2 molecules, respectively. These species could have been trapped in the pores of the HfO_2 film during

https://doi.org/10.1021/acsanm.1c00587
ACS Appl. Nano Mater. XXXX, XXX, XXX−XXX

the deposition process (O_2 from oxygen plasma and N_2 from carrier gas) or, alternatively, adsorbed on the surface of stack structures from the atmosphere.[52,53]

X-ray Photoelectron Spectroscopy. The elemental composition of reference HfO_2 ALD films, as-deposited and graphene-coated, was estimated from XPS survey spectra (not shown) and showed close agreement with stoichiometric hafnium to oxygen content ratios, that is, corresponded to that of HfO_2, for the as-deposited oxide layers without the graphene cover layer, whereas the relative oxygen content was found to be somewhat in excess compared to that in the graphene-coated samples.

However, the main purpose of the application of XPS was to evaluate the presence of possible residual species associated with the PMMA-assisted graphene transfer process, thus probing the quality of the as-transferred graphene layer. XPS can, thereby, provide additional information about surface defects/impurities and have been used for the characterization of nanographite/graphene structures in this regard before.[48] In the present study, the C 1s spectrum from the HfO_2 film covered by the transferred graphene (Figure 6, upper panel)

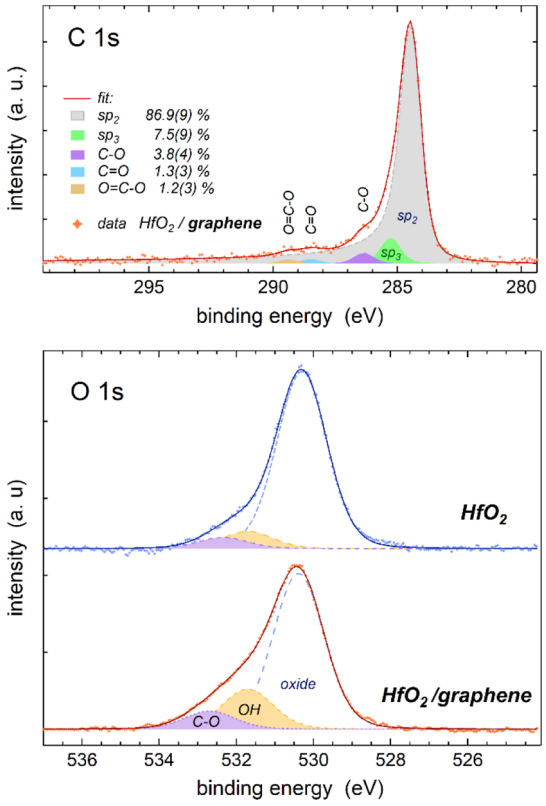

Figure 6. High-resolution XPS scan of the C 1s core-level region with spectral component fit (symbols—data, solid line—overall fit envelope, and colored fields—fit components) upper panel, and high-resolution XPS scan of the O 1s core level peak with decomposed components, measured on the graphene-coated HfO_2 film without the top HfO_2 layer bottom panel.

was fitted in the common manner using the asymmetric Doniach–Sunjic (DS) line shape[32] for the (metallic) sp^2 component characteristic of graphene and Gaussian–Lorentzian symmetric shapes for the other components,[54] after subtracting Shirley background. The asymmetry of the DS line was limited to a value of 0.14, which has earlier been found valid for pristine graphene.[55−57] This was appropriate in order to avoid underestimation of additional, possibly impurity-originated shoulders, and asymmetric shape inadequately dominating in the spectrum, even if some authors have reported that the peak asymmetry can be enhanced in the presence of defects.[56]

Herewith, the purity of graphene was estimated rather conservatively from C 1s XPS analysis and that the residual content found here can be plausibly seen as the upper limit values for the impurities in the sample. The XPS results for the C 1s spectrum (Figure 6, upper panel) indicated that the relative content of what is identified as oxidized carbon remained below 5−6% of the total signal, while the separate (~7.5%) sp^3 feature at least partly associated to dangling bonds at edges of graphene patches.[57] The latter was partially supported by the Raman measurements, described above, which confirmed that the D band was, in practice, absent in the case of graphene not covered by the top HfO_2 layer.

It is worth noting that for the PMMA used in the transferring process of the graphene layer to the oxide surface, even the residue after subtracting the sp^2 component from the C 1s spectrum bears no close resemblance to its C 1s spectrum of PMMA,[58] suggesting that there are virtually no PMMA residues left on graphene in our experiments.

In Figure 6, bottom panel, one can see that the O 1s photoelectron spectrum measured on a HfO_2 film, not coated with transferred graphene, reveals a minor contribution from hydroxyl groups (approximately 9% of the overall oxygen signal), present on the HfO_2 film surface, and from adsorbed hydrocarbons (6%). For the graphene-covered HfO_2 sample, the spectral component referring to the presence of hydrocarbons grew by around 1.5 times in relation to the main oxide peak, which was consistent with the C 1s signal other than that from the sp^2-hybridized carbon signal originating from graphene sheets. At the same time, the dominating lowest binding energy component from the HfO_2 remained consistent with the stoichiometric ratio between oxygen and hafnium in the probed volume, as derived from the signal ratios for both these samples in survey spectra (not shown). However, the middle component at ~531.5 eV binding energy, which commonly originates in surface hydroxyl,[59] grew approximately twice, plausibly originating from the hydroxylated metal oxide surface under the graphene layer. This is also supported by an observation, according to which excessive oxygen-bonded carbon was not present in the C 1s spectrum.

The Hf 4f spectra for both graphene-covered and bare HfO_2 (not shown) could be well fitted by a single spin–orbit split pair of Voigt profiles, hence indicating that the samples were chemically homogeneous, as expected for these thick oxide films.[60] The Hf $4f_{7/2}$ binding energy of 16.9 eV agrees with several previous studies of HfO_2 films[60−62] even if the values closer to 18 eV have also been considered.[63] However, such a divergence of values may stem from the common but lately criticized[64,65] practice of referencing binding energies to adventitious carbon (often still the best available option), which can be circumvented using different internal references, viz., the Si 2p signal for very thin films on such a substrate,[65,66] whose use has previously visualized overcorrection using the carbon reference,[60,66] and raised reconsiderations if the surface carbon is, necessarily, in a sufficiently intimate contact to the surface, providing charge equilibrium with the oxide surface beneath.

https://doi.org/10.1021/acsanm.1c00587
ACS Appl. Nano Mater. XXXX, XXX, XXX−XXX

Resistive Switching Behavior. In order to follow the effect of the graphene layer on electrical properties, selected stacks with graphene and without graphene were subjected to resistive switching measurements. Figure 7 depicts the

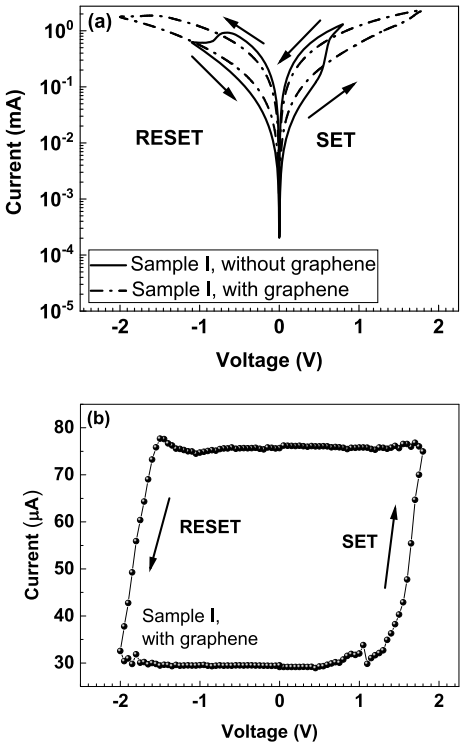

Figure 7. Current–voltage curves of the HfO_2–HfO_2 reference double layers, as well as HfO_2-graphene-HfO_2 stacks (a), and a current–voltage memory map from HfO_2-graphene-HfO_2 stacks (b). The electrode area was 0.002 mm^2. In both double layers and graphene-containing stacks, the first HfO_2 layer was grown in the chloride-based ALD process, and the top HfO_2 layer was grown from the alkylamide precursor (Sample **I**).

switching behavior observed in both types of stacks, where the first HfO_2 layer was grown using $HfCl_4$ and H_2O, whereas the second HfO_2 layer was grown using $Hf[N(C_2H_5)(CH_3)]_2$ and O_2 plasma (Sample **I**, Figure 1). One can see that the switching performance was achieved and repeatable with and without the graphene interlayer between bottom and top HfO_2 films. The conventional resistive switching current–voltage characteristics were measured along with linear voltage sweeps and resulted in uniform switching with a defined high resistivity state (HRS) and low resistivity state (LRS), although the ratio between those states did not exceed 8, that is, did not reach an order of magnitude. The resistive switching behavior observed was bipolar and proceeded counterclockwise. This means that switching from one resistive state to another required a different polarity of the applied voltage. The switching from the HRS to LRS, that is, the SET procedure, occurred during sweeping positive voltage on the Ti electrode in relation to the bottom TiN electrode and, correspondingly, switching from the LRS to HRS, that is, the RESET process took place during the negative voltage sequence.

The bottom and top HfO_2 layers were, as described above, grown in different ALD processes using $HfCl_4$ and $Hf[N(CH_3)(C_2H_5)]_4$ as precursors, respectively. The chloride-based process results in films inevitably containing chlorine as the residual impurity,[20] which was confirmed by XRF in this work as well and remained in the range of 0.6 at. %, whereas the alkylamide-based process results in films containing more carbon.[67] In addition to chemically somewhat different compositions of these films contributing the double-layer stack, the HfO_2 grown from the chloride precursor may form as somewhat more intensely crystallized compared to that formed in the alkylamide process.[20,67] Both structural and chemical differences, that is, process-related discontinuity in the complete stack, plausibly cause energetic barriers of moderate height for charge carriers, in addition to the interfaces between bottom and top oxide layers. This may be a possible reason to the current jump (Figure 7a) during switching events, which in the case of the SET process occurred at +0.6 V and in the case of RESET occurred at −0.7 V.

In the case of the stacked nanostructures with the graphene interlayer, the voltages for SET and RESET appeared somewhat more symmetric and the "humps" were noticeably weakened (Figure 7a). Also decreased was the LRS/HRS ratio, which did not exceed 2.5 in the case of the embedded graphene layer. It is possible that the introduction of naturally conductive graphene with possibly accompanied doping, together with increased defect densities, has significantly decreased the effect of the barrier to the conducting pathways (possibly filaments), suppressing both the stepwise switching process and resistance state differences. Note that the conduction currents through the graphene-containing stack (Figure 7a) were increased by almost an order of magnitude, compared to those measured in the reference HfO_2 stack (Figure 7a).

In connection with the conventional resistive switching measurements, one has to consider that rectangular voltage pulses are applied on the electrodes, with the amplitude increasing along with the number of pulses in sequence. At the increasing voltage pulses, values of current are recorded, which sequentially and cumulatively form the current–voltage curve until the transition (switching) to the LRS. Upon back-and-forth sweeping of the sequence of voltage pulses with gradually and alternately increasing and decreasing amplitudes, the envelope curves of the current–voltage dependences are acquired (Figure 7a), showing typical resistive switching behavior in such a medium. In order to better measure this hysteresis, low reading voltage curves can be recorded, and this means that whenever we increase the applied voltage, the current value is measured at the reading voltage, instead of at the increased voltage value. Such hysteretic curves can be termed hysterons, which demonstrate the nonvolatile effect of the MIM device studied, and improve the distinction between low and high conduction memory states, as was observed also in the present study for the stack containing the graphene interlayer (Figure 7b). In the latter case, currents were read at voltage values of 0.1 V in between the sequential sampling bias voltage pulses. The value of the measured current was, dominantly, determined by the two resistance states achieved alternately. Two clearly defined plateaus were reached and passed through before and after the sequential SET and RESET transitions (Figure 7b). Current–voltage loop with remarkable squareness, alternatively defined as a current memory map, was thus formed with the memory window between the high and low current states (in the present case, with a nominal LRS/HRS ratio of 1.5 only) distinctively separated by 45 μA.

https://doi.org/10.1021/acsanm.1c00587
ACS Appl. Nano Mater. XXXX, XXX, XXX−XXX

The HfO_2-graphene-HfO_2 stacks with HfO_2 films both grown from the $Hf[N(C_2H_5)(CH_3)]_4$ precursor demonstrated resistive switching behavior defined somewhat better compared to that observed in the stacks where the bottom HfO_2 film was grown from $HfCl_4$ and H_2O. The results are exemplified by Figure 8, inset, depicting hysteretic switching behavior of TiN/HfO_2/graphene/HfO_2/Ti nanostructures (Sample **IV**), in which the bottom HfO_2 layer was heat-treated without boiling in water before the graphene transfer process. In Figure 8, inset, the current loops formed during 10 subsequential back-and-forth voltage sweeps are depicted.

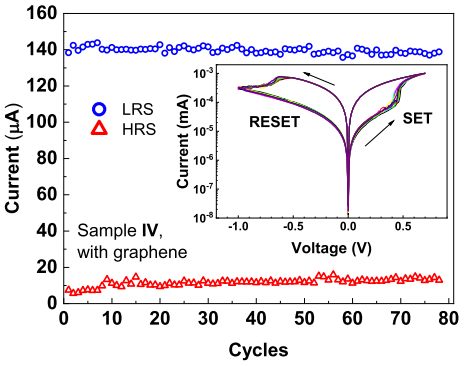

Figure 8. Retention characteristic, measured from the TiN/HfO_2/graphene/HfO_2/Ti (Sample **IV**) stack, where HfO_2 layers were grown using TEMAHf and O_2 plasma. The inset shows 10 sequential current−voltage envelope curves. The electrode dot area was 0.05 mm^2. The retention current values were registered at the voltage values of 0.1 V.

The switching between two distinctive resistivity states took place at approximately 0.5 and −0.6 V in the case of both SET and RESET processes, respectively. The ratio between low- and high-resistance states (LRS/HRS) reached an order of magnitude, that is, 10, approximately, at 0.02 V. Notably, the LRS/HRS ratio remained appreciably stable along with cycling the switching voltages over several tens of times (Figure 8). The latter result could be regarded as promising in terms of the first retention characteristics.

In Figure 9, average resistive switching voltage curves are depicted. These loops are representative for the samples with differently treated HfO_2 surfaces before the graphene transfer process. It is worth noting that the stacks behaved quite similarly in terms of the LRS/HRS ratio and switching voltage values, except the one which has been rinsed in 2-propanol followed by rinsing in water (Sample **V**) (Figure 9). This can be better demonstrated in the memory map comparison of Figure 10. Plausibly, 2-propanol and water treatment has resulted in densification of a layer of the hydrocarbon species in addition to the graphene, giving rise to the electronic defect densities. The latter has, also plausibly, led to the narrower memory window expressed by both the current envelope curve (Figure 9) and current memory map (Figure 10) measured for Sample **V** (Figure 1), when compared to the rest of the samples. As the number of defects increased, the leakage current in the bulk increased. The applied energy was dispersed in the whole bulk, and thus, less energy was employed to form the conductive filaments, making them weaker (less conductive) than in the other cases. As a result, lower currents were obtained in the LRS state of Sample **V**.

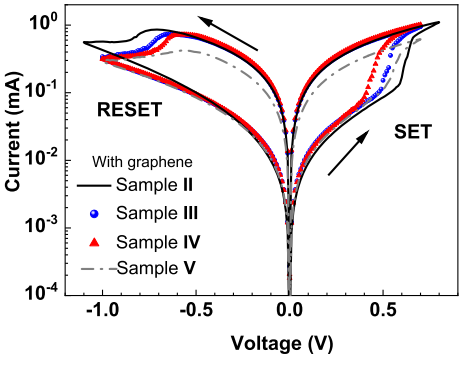

Figure 9. Representative average current−voltage envelope curves measured from the TiN/HfO_2/graphene/HfO_2/Ti stack, where all the HfO_2 layers were grown using TEMAHf and O_2 plasma as precursors. The bottom HfO_2 surface treatment procedures are denoted by the labels presented in the legend in accordance with Figure 1.

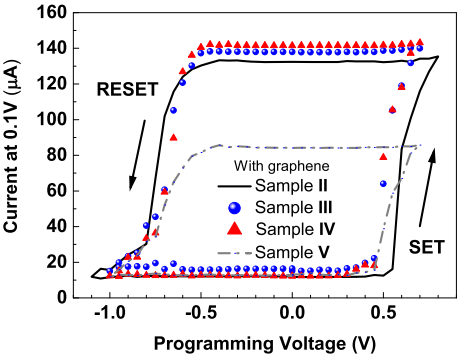

Figure 10. Current−voltage memory maps, measured from TiN/HfO_2/graphene/HfO_2/Ti nanostructures, where all HfO_2 layers were grown using TEMAHf and O_2 plasma. The bottom HfO_2 surface treatment procedures are denoted by the labels within the legend in accordance with Figure 1.

CONCLUSIONS

Chemical vapor-deposited graphene layers were successfully transferred between embedding layers of HfO_2 grown by ALD. The HfO_2 films grown as substrates to graphene were deposited from $HfCl_4$ and water or $Hf[N(CH_3)(C_2H_5)]_4$ and O_2 plasma as precursors, whereby the HfO_2 films on graphene were grown only from $Hf[N(CH_3)(C_2H_5)]_4$ and plasma. Different aging and rinsing treatments were applied prior to both graphene transfer procedures and HfO_2 ALD, in order to improve adhesion of graphene on the bottom HfO_2 layer and nucleation of top HfO_2 on graphene, respectively. Raman probing allowed one to decide that the structure of graphene was essentially retained after the plasma ALD process. However, also in accordance with Raman, defects were created in graphene during plasma ALD of HfO_2, regardless of protective treatment procedures. Nevertheless, after deposition of the upper layer HfO_2, the Raman spectra from the differently treated graphene nanostructures became uniformly similar. The HfO_2 dielectric layers grew homogeneously and were nanocrystalline.

Resistive switching measurements revealed that the HfO_2-graphene-HfO_2 stacks consisting of HfO_2 layers both grown from hafnium alkylamide and O_2 plasma can demonstrate

https://doi.org/10.1021/acsanm.1c00587
ACS Appl. Nano Mater. XXXX, XXX, XXX−XXX

more reliable resistive switching behavior compared to the devices, where the bottom HfO_2 film is deposited from carbon-free chloride and water precursors. In the case of the chloride-based growth process, the application of the graphene barrier between constituent HfO_2 films could somewhat decrease the low- to high-resistance ratio in current−voltage switching loops. The switching behavior remains measurable, nevertheless, and emerges further when recording current−voltage memory maps in the small-signal measurement regime.

All the stacks with both HfO_2 layers grown from $Hf[N(C_2H_5)(CH_3)]_4$ and plasma demonstrated similar resistive switching behavior in terms of current−voltage envelope curves. Thus, despite the variability and options for both oxide surface and graphene treatment procedures, the nanodevice preparation processes have demonstrated appreciable robustness, only moderately affecting the electrical performance. None of the processes applied influenced the graphene or contact layers destructively. Nevertheless, different bottom HfO_2 film surface treatments can have slightly differing effects on the RS behavior. Comparing HfO_2 films grown on TiN substrates and boiled in water with samples prepared after the plate was only heated without water treatment, one could see and may also further expect somewhat lower commutation voltages in both polarities, possibly because the contact between the graphene layer and the substrate may have been further improved. Unequivocally, lower current values in the low-resistance state may be reached after treatments in 2-propanol and water, despite the increase in electronic defect densities, and accompanying higher leakage currents in the high-resistance state. The increased number of defects results in a higher leakage current. This causes the applied energy to be dispersed in the whole bulk. Therefore, the energy actually used to form the conductive filaments decreases, resulting in lower currents in the LRS state.

AUTHOR INFORMATION

Corresponding Author

Tauno Kahro − *Institute of Physics, University of Tartu, 50411 Tartu, Estonia*; orcid.org/0000-0002-8243-902X; Email: tauno.kahro@ut.ee

Authors

Aivar Tarre − *Institute of Physics, University of Tartu, 50411 Tartu, Estonia*

Tanel Käämbre − *Institute of Physics, University of Tartu, 50411 Tartu, Estonia*

Helle-Mai Piirsoo − *Institute of Physics, University of Tartu, 50411 Tartu, Estonia*

Jekaterina Kozlova − *Institute of Physics, University of Tartu, 50411 Tartu, Estonia*; orcid.org/0000-0002-7775-1246

Peeter Ritslaid − *Institute of Physics, University of Tartu, 50411 Tartu, Estonia*; orcid.org/0000-0002-3603-2237

Aarne Kasikov − *Institute of Physics, University of Tartu, 50411 Tartu, Estonia*

Taivo Jõgiaas − *Institute of Physics, University of Tartu, 50411 Tartu, Estonia*

Guillermo Vinuesa − *Department of Electronics, University of Valladolid, 47011 Valladolid, Spain*

Salvador Dueñas − *Department of Electronics, University of Valladolid, 47011 Valladolid, Spain*

Helena Castán − *Department of Electronics, University of Valladolid, 47011 Valladolid, Spain*

Aile Tamm − *Institute of Physics, University of Tartu, 50411 Tartu, Estonia*; orcid.org/0000-0002-0547-0824

Kaupo Kukli − *Institute of Physics, University of Tartu, 50411 Tartu, Estonia*

Complete contact information is available at: https://pubs.acs.org/10.1021/acsanm.1c00587

Notes

The authors declare no competing financial interest.

ACKNOWLEDGMENTS

The present study was partially funded by the European Regional Development Fund project "Emerging orders in quantum and nanomaterials" (TK134), "Advanced materials and high-technology devices for sustainable energetics, sensorics and nanoelectronics" (TK141), Spanish Ministry of Economy and Competitiveness (TEC2017-84321-C4-2-R) with support of Feder funds, and Estonian Research Agency (PRG4, PRG753). Alma-Asta Kiisler is thanked for the assistance in the studies, and Dr. Mihkel Rähn is thanked for the assistance in TEM analysis.

REFERENCES

(1) Lee, S.; Sohn, J.; Jiang, Z.; Chen, H.-Y.; Philip Wong, H.-S. Metal oxide-resistive memory using graphene-edge electrodes. *Nat. Commun.* **2015**, *6*, 8407.

(2) Shen, Z.; Zhao, C.; Qi, Y.; Mitrovic, I. Z.; Yang, L.; Wen, J.; Huang, Y.; Li, P.; Zhao, C. Memristive non-volatile memory based on graphene materials. *Micromachines* **2020**, *11*, 341.

(3) Lee, J.; Du, C.; Sun, K.; Kioupakis, E.; Lu, W. D. Tuning ionic transport in memristive devices by graphene with engineered nanopores. *ACS Nano* **2016**, *10*, 3571.

(4) Mannequin, C.; Delamoreanu, A.; Latu-Romain, L.; Jousseaume, V.; Grampeix, H.; David, S.; Rabot, C.; Zenasni, A.; Vallee, C.; Gonon, P. Graphene-HfO2-based resistive RAM memories. *Microelectron. Eng.* **2016**, *161*, 82.

(5) Hollander, M. J.; LaBella, M.; Hughes, Z. R.; Zhu, M.; Trumbull, K. A.; Cavalero, R.; Snyder, D. W.; Wang, X.; Hwang, E.; Datta, S.; Robinson, J. A. Enhanced transport and transistor performance with oxide seeded high-k gate dielectrics on wafer-scale epitaxial graphene. *Nano Lett.* **2011**, *11*, 3601.

(6) Vervuurt, R. H. J.; Kessels, W. M. M. E.; Bol, A. A. Atomic layer deposition for graphene device integration. *Adv. Mater. Interfaces* **2017**, *4*, 1700232.

(7) Schilirò, E.; Nigro, R.; Lo Nigro, F.; Giannazzo, F. Recent advances in seeded and seed-layer-free atomic layer deposition of high-k dielectrics on graphene for electronics. *J. Carbon Res.* **2019**, *5*, 53.

(8) Giannazzo, F.; Schilirò, E.; Nigro, R.; Lo Nigro, F.; Yakimova, R. Atomic layer deposition of high-k insulators on epitaxial graphene: A review. *Appl. Sci.* **2020**, *10*, 2440.

(9) Jeong, S.-J.; Gu, Y.; Heo, J.; Yang, J.; Lee, C.-S.; Lee, M.-H.; Lee, Y.; Kim, H.; Park, S.; Hwang, S. Thickness scaling of atomic-layer-deposited HfO_2 films and their application to wafer-scale graphene tunnelling transistors. *Sci. Rep.* **2016**, *6*, 20907.

(10) Giambra, M. A.; Benfante, A.; Pernice, R.; Miseikis, V.; Fabbri, F.; Reitz, C.; Pernice, W. H. P.; Krupke, R.; Calandra, E.; Stivala, S.; Busacca, A. C.; Danneau, R. Graphene field-effect transistors employing different thin oxide films: A comparative study. *ACS Omega* **2019**, *4*, 2256.

(11) Kukli, K.; Ritala, M.; Sajavaara, T.; Keinonen, J.; Leskelä, M. Atomic layer deposition of hafnium dioxide films from hafnium tetrakis(ethylmethylamide) and water. *Chem. Vap. Deposition* **2002**, *8*, 199.

(12) Fallahazad, B.; Kim, S.; Colombo, L.; Tutuc, E. Dielectric thickness dependence of carrier mobility in graphene with HfO_2 top dielectric. *Appl. Phys. Lett.* **2010**, *97*, 123105.
(13) Kim, K. S.; Oh, I.-K.; Jung, H.; Kim, H.; Yeom, G. Y.; Kim, K. N. Atomic layer deposition of HfO_2 on graphene through controlled ion beam treatment. *Appl. Phys. Lett.* **2016**, *108*, 213102.
(14) Zheng, L.; Cheng, X.; Cao, D.; Wang, Z.; Xu, D.; Xia, C.; Shen, L.; Yu, Y. HfO_2 dielectric film growth directly on graphene by H_2O-based atomic layer deposition. *J. Vac. Sci. Technol., A* **2014**, *32*, 01A103.
(15) Zheng, L.; Cheng, X.; Yu, Y.; Xie, Y.; Li, X.; Wang, Z. Controlled direct growth of Al_2O_3-doped HfO_2 films on graphene by H_2O-based atomic layer deposition. *Phys. Chem. Chem. Phys.* **2015**, *17*, 3179.
(16) Grebel, H.; Stan, L.; Sumant, A.; Liu, Y.; Gosztola, D.; Ocola, L.; Fisher, B. Transfer of graphene with protective oxide layers. *ChemEngineering* **2018**, *2*, 58.
(17) Alivio, T. E. G.; De Jesus, L. R.; Dennis, R. V.; Jia, Y.; Jaye, C.; Fischer, D. A.; Singisetti, U.; Banerjee, S. Atomic layer deposition of hafnium(IV) oxide on graphene oxide: Probing interfacial chemistry and nucleation by using X-ray absorption and photoelectron spectroscopies. *ChemPhysChem* **2015**, *16*, 2842.
(18) Xiao, M.; Qiu, C.; Zhang, Z.; Peng, L.-M. Atomic-layer-deposition growth of an ultrathin HfO_2 film on graphene. *ACS Appl. Mater. Interfaces* **2017**, *9*, 34050.
(19) Shin, J. W.; Kang, M. H.; Oh, S.; Yang, B. C.; Seong, K.; Ahn, H.-S.; Lee, T. H.; An, J. Atomic layer deposited high-k dielectric on graphene by functionalization through atmospheric plasma treatment. *Nanotechnology* **2018**, *29*, 195602.
(20) Kukli, K.; Aarik, J.; Ritala, M.; Uustare, T.; Sajavaara, T.; Lu, J.; Sundqvist, J.; Aidla, A.; Pung, L.; Hårsta, A.; Leskelä, M. Effect of selected atomic layer deposition parameters on the structure and dielectric properties of hafnium oxide films. *J. Appl. Phys.* **2004**, *96*, 5298.
(21) Alles, H.; Aarik, J.; Aidla, A.; Fay, A.; Kozlova, J.; Niilisk, A.; Pärs, M.; Rähn, M.; Wiesner, M.; Hakonen, P.; Sammelselg, V. Atomic layer deposition of HfO_2 on graphene from $HfCl_4$ and H_2O. *Cent. Eur. J. Phys.* **2011**, *9*, 319.
(22) Oh, I.-K.; Tanskanen, J.; Jung, H.; Kim, K.; Lee, M. J.; Lee, Z.; Lee, S.-K.; Ahn, J.-H.; Lee, C. W.; Kim, K.; Kim, H.; Lee, H.-B. -R. Nucleation and Growth of the HfO_2 Dielectric Layer for Graphene-Based Devices. *Chem. Mater.* **2015**, *27*, 5868.
(23) Kim, K.-M.; Jang, J. S.; Yoon, S.-G.; Yun, J.-Y.; Chung, N.-K. Structural, optical and electrical properties of HfO_2 thin films deposited at low-temperature using plasma-enhanced atomic layer deposition. *Materials* **2020**, *13*, 2008.
(24) Yang, T.; Wang, H.; Zhang, B.; Yan, X. Enhanced memory characteristics of charge trapping memory by employing graphene oxide quantum dots. *Appl. Phys. Lett.* **2020**, *116*, 103501.
(25) El-Atab, N.; Turgut, B. B.; Okyay, A.; Nayfeh, A. Graphene nanoplatelets embedded in HfO_2 for MOS memory. *ECS Trans.* **2015**, *66*, 39.
(26) Arroval, T.; Aarik, L.; Rammula, R.; Kruusla, V.; Aarik, J. Effect of substrate-enhanced and inhibited growth on atomic layer deposition and properties of aluminum−titanium oxide films. *Thin Solid Films* **2016**, *600*, 119.
(27) Granneman, E.; Fischer, P.; Pierreux, D.; Terhorst, H.; Zagwijn, P. Batch ALD: Characteristics, comparison with single wafer ALD, and examples. *Surf. Coat. Technol.* **2007**, *201*, 8899.
(28) Zagwijn, P. M.; Verweij, W.; Pierreux, D.; Adjeroud, N.; Bankras, R.; Oosterlaken, E.; Snijders, G. J.; van den Hout, M.; Fischer, P.; Wilhelm, R.; Knapp, M. Novel batch titanium nitride CVD process for advanced metal electrodes. *ECS Trans.* **2008**, *13*, 459.
(29) Liang, X.; Sperling, B. A.; Calizo, I.; Cheng, G.; Hacker, C. A.; Zhang, Q.; Obeng, Y.; Yan, K.; Peng, H.; Li, Q.; Zhu, X.; Yuan, H.; Hight Walker, A. R.; Liu, Z.; Peng, L.-m.; Richter, C. A. Toward Clean and Crackless Transfer of Graphene. *ACS Nano* **2011**, *5*, 9144−9153.
(30) Goniszewski, S.; Adabi, M.; Shaforost, O.; Hanham, S. M.; Hao, L.; Klein, N. Correlation of p-doping in CVD Graphene with Substrate Surface Charges. *Sci. Rep.* **2016**, *6*, 22858.
(31) Fairley, N. *CasaXPS: Processing Software for XPS, AES, SIMS and More*; Casa Software Ltd., 2018 [online] http://www.casaxps.com/.
(32) Doniach, S.; Sunjic, M. Many-electron singularity in X-ray photoemission and X-ray line spectra from metals. *J. Phys. C: Solid State Phys.* **1970**, *3*, 285.
(33) Kukk, E.; Snell, G.; Bozek, J. D.; Cheng, W.-T.; Berrah, N. Vibrational structure and partial rates of resonant Auger decay of theN1s→2πcore excitations in nitric oxide. *Phys. Rev. A: At., Mol., Opt. Phys.* **2001**, *63*, 062702.
(34) Kukk, E.; Ueda, K.; Hergenhahn, U.; Liu, X.-J.; Prümper, G.; Yoshida, H.; Tamenori, Y.; Makochekanwa, C.; Tanaka, T.; Kitajima, M.; Tanaka, H. Violation of the Franck-Condon Principle due to Recoil Effects in High Energy Molecular Core-Level Photoionization. *Phys. Rev. Lett.* **2005**, *95*, 133001.
(35) Kahro, T.; Castán, H.; Dueñas, S.; Merisalu, J.; Kozlova, J.; Jõgiaas, T.; Piirsoo, H.-M.; Kasikov, A.; Ritslaid, P.; Mändar, H.; Tarre, A.; Tamm, A.; Kukli, K. Structure and behavior of ZrO_2/graphene/ZrO_2 stacks. *J. Vac. Sci. Technol., A* **2020**, *38*, 063411.
(36) Beams, R.; Gustavo Cançado, L.; Novotny, L. Raman characterization of defects and dopants in graphene. *J. Phys.: Condens. Matter* **2015**, *27*, 083002.
(37) Ferrari, A. C.; Basko, D. M. Raman spectroscopy as a versatile tool for studying the properties of graphene. *Nat. Nanotechnol.* **2013**, *8*, 235.
(38) Casiraghi, C.; Pisana, S.; Novoselov, K. S.; Geim, A. K.; Ferrari, A. C. Raman fingerprint of charged impurities in graphene. *Appl. Phys. Lett.* **2007**, *91*, 233108.
(39) Yin, Y.; Cheng, Z.; Wang, L.; Jin, K.; Wang, W. Graphene, a material for high temperature devices − intrinsic carrier density, carrier drift velocity, and lattice energy. *Sci. Rep.* **2014**, *4*, 5758.
(40) Hao, Q.; Morton, S. M.; Wang, B.; Zhao, Y.; Jensen, L.; Jun Huang, T. Tuning surface-enhanced Raman scattering from graphene substrates using the electric field effect and chemical doping. *Appl. Phys. Lett.* **2013**, *102*, 011102.
(41) Ben Maad, Y.; Durnez, A.; Ajlani, H.; Madouri, A.; Oueslati, M.; Meftah, A. Modulation of electron transfer in Si/SiO_2/HfO_2/Graphene by the thickness. *Appl. Phys. A* **2020**, *126*, 754.
(42) Ryu, S.; Liu, L.; Berciaud, S.; Yu, Y.-J.; Liu, H.; Kim, P.; Flynn, G. W.; Brus, L. E. Atmospheric Oxygen Binding and Hole Doping in Deformed Graphene on a SiO_2 Substrate. *Nano Lett.* **2010**, *10*, 4944−4951.
(43) Liu, D.; He, M.; Huang, C.; Sun, X.; Gao, B. Fermi-Level Dependence of the Chemical Functionalization of Graphene with Benzoyl Peroxide. *J. Phys. Chem. C* **2017**, *121*, 10546−10551.
(44) Kim, S.-Y.; Kim, Y. J.; Jung, U.; Lee, B. H. Chemically induced Fermi level pinning effects of high-k dielectrics on graphene. *Sci. Rep.* **2018**, *8*, 2992.
(45) Ni, Z. H.; Wang, H. M.; Luo, Z. Q.; Wang, Y. Y.; Yu, T.; Wu, Y. H.; Shen, Z. X. The effect of vacuum annealing on graphene. *J. Raman Spectrosc.* **2010**, *41*, 479.
(46) Cançado, L. G.; Jorio, A.; Martins Ferreira, E. H.; Stavale, F.; Achete, C. A.; Capaz, R. B.; Moutinho, M. V. O.; Lombardo, A.; Kulmala, T. S.; Ferrari, A. C. Quantifying Defects in Graphene via Raman Spectroscopy at Different Excitation Energies. *Nano Lett.* **2011**, *11*, 3190−3196.
(47) Wang, Q. H.; Jin, Z.; Kim, K. K.; Hilmer, A. J.; Paulus, G. L. C.; Shih, C.-J.; Ham, M.-H.; Sanchez-Yamagishi, J. D.; Watanabe, K.; Taniguchi, T.; Kong, J.; Jarillo-Herrero, P.; Strano, M. S. Understanding and controlling the substrate effect on graphene electron-transfer chemistry via reactivity imprint lithography. *Nat. Chem.* **2012**, *4*, 724.
(48) Ganesan, K.; Ghosh, S.; Gopala Krishna, N.; Ilango, S.; Kamruddin, M.; Tyagi, A. K. A comparative study on defect estimation using XPS and Raman spectroscopy in few layer

https://doi.org/10.1021/acsanm.1c00587
ACS Appl. Nano Mater. XXXX, XXX, XXX−XXX

nanographitic structures. *Phys. Chem. Chem. Phys.* **2016**, *18*, 22160−22167.
(49) Xiao, M.; Qiu, C.; Zhang, Z.; Peng, L.-M. Atomic-Layer-Deposition Growth of an Ultrathin HfO2 Film on Graphene. *ACS Appl. Mater. Interfaces* **2017**, *9*, 34050−34056.
(50) Jorio, A.; Ferreira, E. H. M.; Moutinho, M. V. O.; Stavale, F.; Achete, C. A.; Capaz, R. B. Measuring disorder in graphene with the G and D bands. *Phys. Status Solidi B* **2010**, *247*, 2980−2982.
(51) Neumann, C.; Reichardt, S.; Venezuela, P.; Drögeler, M.; Banszerus, L.; Schmitz, M.; Watanabe, K.; Taniguchi, T.; Mauri, F.; Beschoten, B.; Rotkin, S. V.; Stampfer, C. Raman spectroscopy as probe of nanometer-scale strain variations in graphene. *Nat. Commun.* **2015**, *6*, 8429.
(52) Kajihara, K.; Hirano, M.; Takimoto, Y.; Skuja, L.; Hosono, H. Diffusion of nitrogen molecules in amorphous SiO_2. *Appl. Phys. Lett.* **2007**, *91*, 071904.
(53) Chow, K. K.; Short, M.; Lam, S.; McWilliams, A.; Zeng, H. A Raman cell based on hollow core photonic crystal fiber for human breath analysis. *Med. Phys.* **2014**, *41*, 092701.
(54) Ferrah, D.; Renault, O.; Petit-Etienne, C.; Okuno, H.; Berne, C.; Bouchiat, V.; Cunge, G. XPS investigations of graphene surface cleaning using H_2- and Cl_2-based inductively coupled plasma. *Surf. Interface Anal.* **2016**, *48*, 451−455.
(55) Kovtun, A.; Jones, D.; Dell'Elce, S.; Treossi, E.; Liscio, A.; Palermo, V. Accurate chemical analysis of oxygenated graphene-based materials using X-ray photoelectron spectroscopy. *Carbon* **2019**, *143*, 268.
(56) Yang, D.-Q.; Sacher, E. Carbon 1s X-ray Photoemission Line Shape Analysis of Highly Oriented Pyrolytic Graphite: The Influence of Structural Damage on Peak Asymmetry. *Langmuir* **2006**, *22*, 860−862.
(57) Estrade-Szwarckopf, H. XPS photoemission in carbonaceous materials: A "defect" peak beside the graphitic asymmetric peak. *Carbon* **2004**, *42*, 1713−1721.
(58) Cunge, G.; Ferrah, D.; Petit-Etienne, C.; Davydova, A.; Okuno, H.; Kalita, D.; Bouchiat, V.; Renault, O. Dry efficient cleaning of poly(methyl methacrylate) residues from graphene with high-density H_2 and H_2-N_2 plasmas. *J. Appl. Phys.* **2015**, *118*, 123302.
(59) Yamamoto, S.; Bluhm, H.; Andersson, K.; Ketteler, G.; Ogasawara, H.; Salmeron, M.; Nilsson, A. In situ x-ray photoelectron spectroscopy studies of water on metals and oxides at ambient conditions. *J. Phys.: Condens. Matter* **2008**, *20*, 184025.
(60) Sammelselg, V.; Rammula, R.; Aarik, J.; Kikas, A.; Kooser, K.; Käämbre, T. XPS and AFM investigation of hafnium dioxide thin films prepared by atomic layer deposition on silicon. *J. Electron Spectrosc. Relat. Phenom.* **2007**, *156−158*, 150−154.
(61) Park, J.; Back, T.; Fairchild, S. B.; Mitchel, W. C.; Elhamri, S.; Boeckl, J.; Martinotti, D.; Douillard, L.; Soukiassian, P. Direct graphene growth on transitional metal with solid carbon source and its converting into graphene/transitional metal oxide heterostructure. *Carbon* **2017**, *116*, 303−309.
(62) Carta, G.; El Habra, N.; Rossetto, G.; Torzo, G.; Crociani, L.; Natali, M.; Zanella, P.; Cavinato, G.; Matterello, V.; Rigato, V.; Kaciulis, S.; Mezzi, A. Growth of hafnium dioxide thin films by MOCVD using a new series of cyclopentadienyl hafnium compounds. *Chem. Vap. Deposition* **2007**, *13*, 626−632.
(63) *NIST X-ray Photoelectron Spectroscopy Database, NIST Standard Reference Database Number 20*; National Institute of Standards and Technology: Gaithersburg MD, 20899, 2000.
(64) Jacquemin, M.; Genet, M. J.; Gaigneaux, E. M.; Debecker, D. P. Calibration of the X-Ray Photoelectron Spectroscopy Binding Energy Scale for the Characterization of Heterogeneous Catalysts: Is Everything Really under Control? *ChemPhysChem* **2013**, *14*, 3618−3626.
(65) Greczynski, G.; Hultman, L. X-ray photoelectron spectroscopy: Towards reliable binding energy referencing. *Prog. Mater. Sci.* **2020**, *107*, 100591.
(66) Lim, Z. H.; Quackenbush, N. F.; Penn, A. N.; Chrysler, M.; Bowden, M.; Zhu, Z.; Ablett, J. M.; Lee, T.-L.; LeBeau, J. M.; Woicik, J. C.; Sushko, P. V.; Chambers, S. A.; Ngai, J. H. Charge Transfer and Built-in Electric Fields between a Crystalline Oxide and Silicon. *Phys. Rev. Lett.* **2019**, *123*, 026805.
(67) Kukli, K.; Ritala, M.; Sajavaara, T.; Keinonen, J.; Leskelä, M. Atomic Layer Deposition of Hafnium Dioxide Films from Hafnium Tetrakis(ethylmethylamide) and Water. *Chem. Vap. Deposition* **2002**, *8*, 199−204.

https://doi.org/10.1021/acsanm.1c00587
ACS Appl. Nano Mater. XXXX, XXX, XXX−XXX